Computational Aerodynamics Study on Neo-Ptero Micro Unmanned Aerial Vehicle

N. I. Ismail
Faculty of Mechanical Engineering, Universiti Teknologi MARA Cawangan Pulau Pinang

Sharudin, Hazim
Faculty of Mechanical Engineering, Universiti Teknologi MARA Cawangan Pulau Pinang

Mahadzir M. M
Faculty of Mechanical Engineering, Universiti Teknologi MARA Cawangan Pulau Pinang

Zurriati M. Ali
Faculty of Mechanical Engineering, Universiti Teknologi MARA

他

https://doi.org/10.5109/4480726

出版情報：Evergreen. 8 (2), pp.438-444, 2021-06. Transdisciplinary Research and Education Center for Green Technologies, Kyushu University
バージョン：

Computational Aerodynamics Study on Neo-Ptero Micro Unmanned Aerial Vehicle

N. I. Ismail[1,2*], Hazim Sharudin[1,2], Mahadzir M. M.[1], Zurriati M. Ali[3]
A. A. Shariffuddin[4] & N.I. Kamel[4]

[1]Faculty of Mechanical Engineering, Universiti Teknologi MARA
Cawangan Pulau Pinang, Pulau Pinang, Malaysia

[2]Creative and Innovation Research Group in Automotive and Aviation (CIRAA), Universiti Teknologi MARA Cawangan Pulau Pinang, Pulau Pinang, Malaysia

[3]Faculty of Mechanical Engineering, Universiti Teknologi MARA, Masai, Johor, Malaysia

[4]IFCON Technology (M) Sdn. Bhd, Taman Industri Meranti Jaya, 47120 Puchong, Selangor

*Author to whom correspondence should be addressed:
E-mail: iswadi558@uitm.edu.my

(Received January 7, 2021; Revised April 26, 2021; accepted April 26, 2021).

Abstract: This work aims to characterize the lift (C_L) and drag (C_D) coefficient distributions on the current Neo-Ptero micro-UAV prototype. A C_L analysis on Neo-Ptero shows that the model has a promising C_L performance throughout the α increment. For every 2° angle of attack increment, the model can generate approximately 22% increment in C_L magnitude. Neo-Ptero also has a decent magnitude in maximum lift coefficient and stall angle at 1.24 and 18°, respectively. C_L comparison works reveal that Neo-Ptero performs better than the other micro-UAV model produce by Ming from National University of Singapore (NUS) and also Serindit (produced by UAV team from University Riau, Indonesia) particularly in terms of α range and C_{Lmax} magnitudes. However, Neo-Ptero suffers from severe C_D generation by producing an average of 23.8% rise in C_D magnitude for every 2° angle of attack increment. A C_D comparison study in performance reveals that compared with other micro-UAV models, Neo-Ptero induces at least 13.2% and 5% larger C_D magnitude and C_D increment, respectively

Keywords: Neo-Ptero UAV; micro unmanned air vehicle; aerodynamics

1. Introduction

Micro-unmanned aerial vehicles (micro-UAVs) are a small autonomous aircraft class that provides an alternative way for data gathering, particularly for confined space areas or low-altitude flights. Micro-UAVs are classified on the basis of their wing lifting design, that is, either the fixed-wing[1)] or rotary-wing[2,3)] design. Both designs have been widely implemented in geometric and photogrammetric[4)] data collection, especially in military, surveillance, reconnaissance, and mapping applications[5)]. In standard mapping missions, fixed-wing micro-UAVs may offer better capability than the rotary-wing counterpart in terms of coverage area and payload compatibility[6)]. In general, the fixed-wing micro-UAV structure can be divided into conventional tail or tailless[7)] configurations. eBee[8)], Pacflyer S100[9)], KS -1[10)], Skywalker X8[10)], and DATAhawk[11)] are some examples of tailless micro-UAV designs that are popularly used for mapping missions. Given its simple structure, light weight, and mobile and rapid deployment, tailless micro-UAVs offer better options than conventional tail micro-UAVs[12)]. Despite their prevalent usage, the aerodynamic performance of these tailless micro-UAV models remains unknown or has yet to be officially released by the developers.

Neo-Ptero[13)] (as shown in Fig. 1) is the latest micro-UAV prototype inspired by the tailless micro-UAV configuration fully developed by IFCON (Malaysia) Private Limited. The tailless micro-UAV prototype was created by using a cutting-edge CNC foam cutter machine based on expanded polypropylene lightweight structure material[14)]. Some Neo-Ptero parts were also developed by using ABS plastic material through 3D printing processes.

The Neo-Ptero structure has a 1.2 m wingspan with a gross weight of 1 kg. For the ready-to-fly prototype, Neo-Ptero is equipped with standard electronic flight control components, such as an electronic speed controller, a transmitter, a brushless motor, a propeller, a battery, and a micro servo, for the proposed flight testing[13)]. The Neo-Ptero micro-UAV model adopts elevon control surfaces

for flight control in which the pitching and rolling motions of the micro-UAV model is controlled on the basis of left and right elevon-deflections[15]. Based on a series of flight tests, Neo-Ptero can fly excellently under stable conditions, with minimal pilot correction input[13].

Despite its successful prototyping and development, the developer is still looking further to improve the flight performance and endurance of Neo-Ptero[13]. Optimizing the lift and drag distribution on Neo-Ptero is seen as a possible method to enhance its overall flight performance. Therefore, understanding the aerodynamic performance of the current Neo-Ptero prototype is crucial for the progress of current micro-UAV configuration. Elucidating the lift and drag performance on the existing Neo-Ptero platform could provide an essential platform for further enhancement action. Thus, this study aims to understand the lift and drag coefficient distributions on the current Neo-Ptero prototype. The study reveals Neo-Ptero's overall lift distribution (C_L) toward the angle of attack (α) changes alongside its maximum lift value, stall angle, and zero-lift angle magnitude. The drag study on Neo-Ptero focuses on its minimum drag coefficient points (C_{Dmin}) and its percentage of drag increment toward the α changes.

To achieve the objective, the study is mainly conducted on the basis of a virtual wind tunnel simulation method (i.e., CFD). Thus, the current work is mainly focused on the computational aerodynamic outcome on the Neo-Ptero platform. In this work, the Neo-Ptero micro-UAV prototype is initially redrawn and converted into a 3D model by using commercial 3D design software. The completed Neo-Ptero 3D model is then imported into the CFD simulation environment for virtual wind tunnel analysis. To ensure that the simulation results are generally acceptable, the lift and drag coefficient distributions on the current Neo-Ptero prototype are compared with other UAVs of the same class.

2. Methodology

2.1 Neo-Ptero 3D Model

The 3D modeling of Neo-Ptero is the first step taken before the virtual wind tunnel analysis. Here, the Neo-Ptero prototype was carefully redrawn to maintain accuracy and consistency with the actual model. Fig. 2 shows the plan view dimension for the 3D model of the Neo-Ptero micro-UAV. The 3D model retains Neo-Ptero's original fuselage profile (BE50)[13] with the wing identically swept backward at 20°. The aspect ratio value between the 3D and actual models was also maintained at 3.46. The wing has a BE50 cambered profile with root, and the tip chords were similarly dimensioned at 341.84 mm[13]. The wingtip components at the wing edge were also retained as the original dimension, as shown in Fig. 3. The control surfaces on the right and left wings were fixed at neutral positions to ensure that the lift and drag distributions were solely contributed by the neutral wing position and were not affected by control surface deflections. In this study, the flight components that contributed to flow complexities[16] and problematic grid generations (e.g., propeller, servo horns, motor mounting, and linkages) were intentionally removed to ensure that the lift and drag distributions were only contributed by Neo-Ptero's fuselage–wing configurations. Fig 4 presents the complete 3D model of the Neo-Ptero micro-UAV.

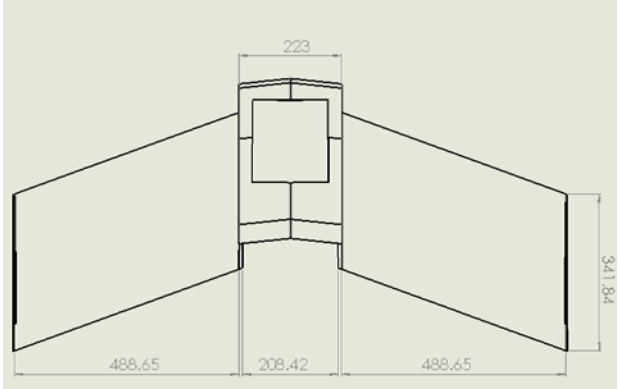

Fig. 2: Neo-Ptero dimension in mm (plan view)

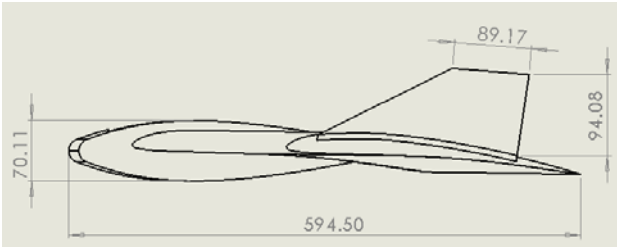

Fig. 3: Neo-Ptero dimension in mm (side view)

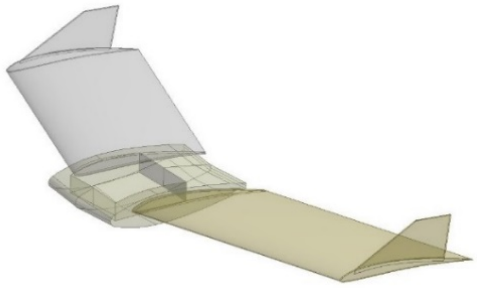

Fig. 4: 3D model of Neo-Ptero

2.2 Airflow Domain Size

The airflow domain was built surrounding the Neo-Ptero 3D model for virtual wind tunnel analysis. Given the symmetrical Neo-Ptero design, the symmetrical boundary condition was fully applied in the airflow domain sizing and the 3D Neo-Ptero model. Thus, both models were sliced into half, as shown in Fig. 5. Such condition was also applied to avoid the computational burden during the mathematical solving step. The overall dimension for the airflow domain is shown in Fig. 5. The airflow domain size is based on Neo-Ptero's total chordwise length (L), where L = 594.50 mm. The coordinate system origin was fixed at the fuselage's

outmost point (leading edge), where the x-, z-, and y-axis were defined in chordwise, spanwise, and normal to the wing direction, respectively.

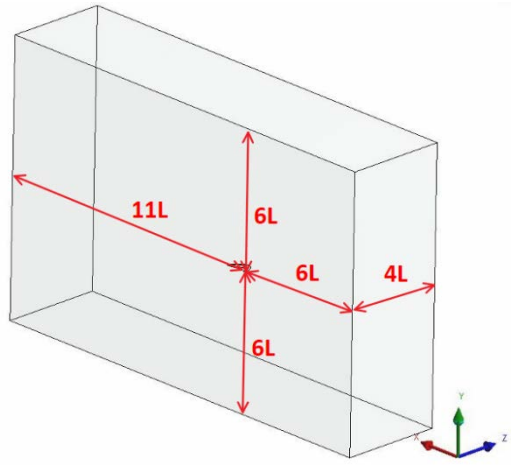

Fig. 5: Airflow domain size

2.3 Mesh Generation and Boundary Conditions

The CFD mesh for the airflow domain was generated on the basis of unstructured hybrid 3D elements. Intense inflation layers were also applied to the elements adjacent to the model surface, as shown in Fig. 6. The y+ magnitude for the first cell above the model surface was conserved at below 1 (y+ <1) to capture the boundary layer effects[17,18]. A grid independence study was conducted to discover the optimum grid size for the present study. For the grid independence study, the simulation was run at Neo-Ptero's cruise speed of 14 m/s and maintained at a medium angle of attack (α) value of 12° to avoid the influence of the stall phenomenon. Five different levels of grid sizes, as summarized in Table 1, were tested to determine the effect of mesh total number on the calculated C_L and C_D magnitudes. The results show insignificant changes in C_L and C_D magnitude beyond the total grid of 1,181,503 elements, as shown in Fig. 6. Therefore, for the present study, the total mesh elements of 1,181,503 was used in all the simulations.

Table 1. Summary of Grid Independence Study

Total Number of Mesh Element	Parameters	
	C_L	C_D
331,521	0.66944	0.08151
612,549	0.83427	0.10419
1,181,503	1.01431	0.12330
1,626,418	1.04557	0.1321
2,315,815	1.00214	0.11787

The boundary conditions applied for the airflow domain is depicted in Fig. 7. The inlet flow condition was enforced at the side and bottom boundaries. Thus, the velocity inlet applied on the boundaries is represented by Eqs. 1 and 2.

$$U_x = U * \cos\alpha, \qquad (1)$$

$$U_y = U * \sin\alpha, \qquad (2)$$

where α is the angle of attack value, and U is inlet velocity set at 14m/s.

The 14 m/s freestream velocity magnitude is equivalent to Neo-Ptero's cruise speed during the flight tests. The α variation was set at -10° to 22° with a 2° interval. To ensure the airflow continuities in the domain, zero-pressure conditions were applied to the outlet boundaries. The Neo-Ptero surface was modeled as no-slip surfaces with automatic wall function was fully implemented to capture the viscous effects. The virtual wind tunnel simulations ran under steady-state conditions with a 5% turbulence intensity setting. Here, the solver used the incompressible flow Navier–Stokes equations with the efficient shear stress turbulence (SST) model to predict the stall phenomenon[19]. The simulation convergence was carefully monitored based on the lift and drag coefficient magnitudes. The momentum residual value was also used to support the reliability of simulation results by setting the magnitude below than 1.0 $\times 10^{-6}$.

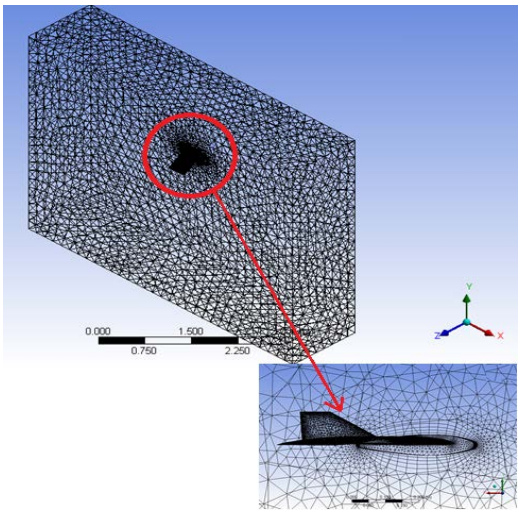

Fig. 6: Optimized grid on airflow domain.

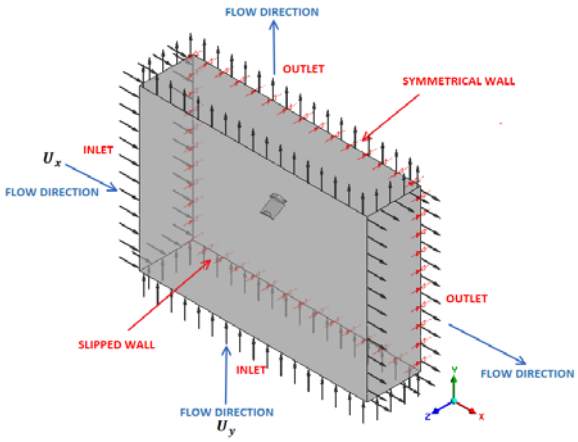

Fig. 7: Boundary conditions applied to the airflow domain.

3. Results

The aerodynamic result analysis of the Neo-Ptero micro-UAV is divided into three main sections. The first two sections focus on the lift and drag performance of the Neo-Ptero itself. The Neo-Ptero's main lift distribution and characteristics, such as the percentage of lift increment (toward the α changes), zero-lift angle, stall angle, and maximum lift coefficient, are presented here. Neo-Ptero's drag performance focuses more on the minimum C_D magnitude (C_{Dmin}) and the percentage of drag increment toward the α changes. In the third section, the lift and drag performance of Neo-Ptero are compared with that of other micro-UAVs of the same class (i.e., NUS[20], Serindit[21], and Hawkeye[22]**)**. This comparative study is conducted to elucidate the Neo-Ptero's aerodynamic level with other micro-UAV models. It is also an initial step to show that the simulation outcomes are generally acceptable and comparable with other micro-UAV models, especially in terms of lift and drag coefficient distributions. The selection of these micro-UAV models is based on their aerodynamic data availability and the similarity of flight envelope between the micro-UAV models. The comparative study focuses on the main lift and drag performance characteristics.

3.1 Lift Performances of Neo-Ptero

Fig. 8 exhibits the C_L performance of the Neo-Ptero micro-UAV. Overall, Neo-Ptero generates almost a linear C_L curve trend toward the α increment. However, a slight nonlinear C_L pattern is exhibited at the α magnitude between -10° and -2°. At this α stage, Neo-Ptero produces the largest percentage of C_L increment with a magnitude of up to 180% for every 2° angle of attack increment. Here, the zero-lift angle of attack ($\alpha_{CL=0}$) for Neo-Ptero is also found at $\alpha_{CL=0}$ = -2°.

As α increases from α = 0° to α = 16°, the C_L curve is found to be in a linear trend. However, the percentage of C_L increment is gradually reduced to 22% for every 2° angle of attack increment.

The C_L curve trend starts to plateau after α = 15°. At α = 15° to18°, the C_L increment drastically decreases to 2% for every 2° angle of attack increment. Such performance indicates that the stall phenomenon has started to dominate the Neo-Ptero surface before the C_L curve climax at its stall angle marked at α_{stall} = 18°. At the stall angle (α_{stall}=18°), Neo-Ptero produces its maximum C_L magnitude at C_{Lmax} = 1.24.

As α increases beyond its stall angle (α = 18°), a sudden drop in C_L trend, in which the magnitude of C_L drastically deteriorates at a rate of - 3% for every 2° angle of attack increment, occurs. Here, one can presume that the stall phenomenon with a significant drag increase has overwhelmed Neo-Ptero's lift distribution[23].

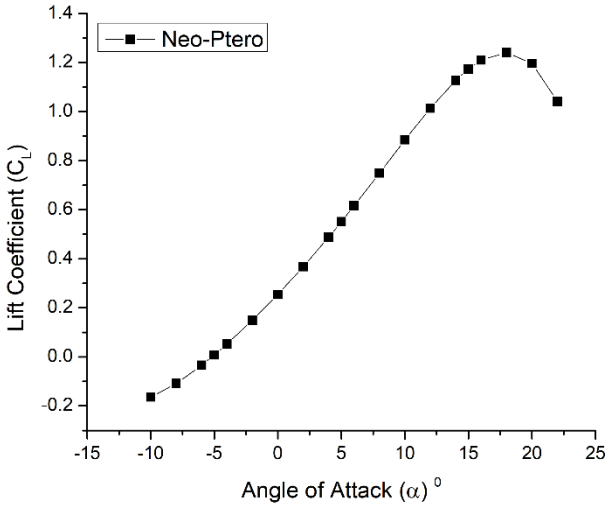

Fig. 8: C_L performances for Neo-Ptero micro-UAV.

3.2 Drag Coefficient of Neo-Ptero

Fig. 9 presents the C_D performance of the Neo-Ptero micro-UAV throughout the α range. Overall, the C_D trend is similar to the common drag trend for an aircraft. The C_D curve starts at a low value and reaches its minimum C_D magnitude here before a drastic C_D increase as α increases further.

At α = -10° to 0°, the C_D magnitude starts at a low magnitude, which is between 0.0398 and 0.0168. At this stage, the percentage of C_D increment has an average of -12%. Here, one can find that Neo-Ptero generates its minimum C_D value (C_{Dmin}) at 0° with C_{Dmin} = 0.0168.

Starting from α = 0° to α = 8°, Neo-Ptero has a severe increase in C_D magnitude. Here, the model has averagely produced a 33.2% increment in C_D magnitude for every 2° angle of attack increment. The ascending trend of C_D magnitude continues at the next α stage (α = 8° to 16°) where the model has averagely induced approximately 23.8% increment in C_D magnitude for every 2° angle of attack increment. At stall angle (α_{stall} = 18°), the C_D magnitude for Neo-Ptero is 0.2435.

As α increases beyond the stall angle (α_{stall} = 18°), the rise of C_D magnitude continues to intensify with an average increment of 21.2% for every 2° angle of attack increment. At this stage, one can presume that the stall phenomenon has overwhelmed the aircraft surface by inducing substantial drag. Such condition provides evidence behind the drastic deterioration of lift performance as α increases beyond the stall angle.

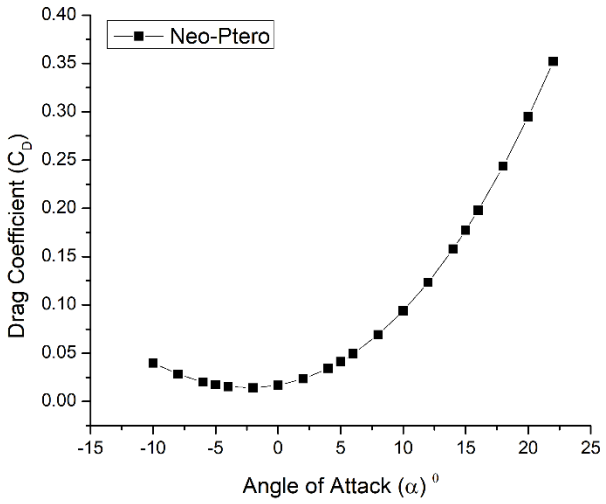

Fig. 9: C_D performances for Neo-Ptero micro-UAV.

3.3 Comparison of Lift and Drag Performances with other micro-UAV models.

A comparative study between Neo-Ptero and other micro-UAV models was conducted to clarify the level of aerodynamic performance produced by the model. These results generally show that the current simulation method can produce results that are acceptable and comparable with that of other micro-UAVs of the same class. Fig. 10 presents the C_L performance of Neo-Ptero alongside with NUS[20], Serindit[21], and Hawkeye[22]. In general, the result shows that the C_L performance of the Neo-Ptero model is comparable with other micro-UAV models in terms of overall C_L distribution, α range, $\alpha_{CL=0}$, $C_{Lmax,}$, and α_{stall} magnitudes.

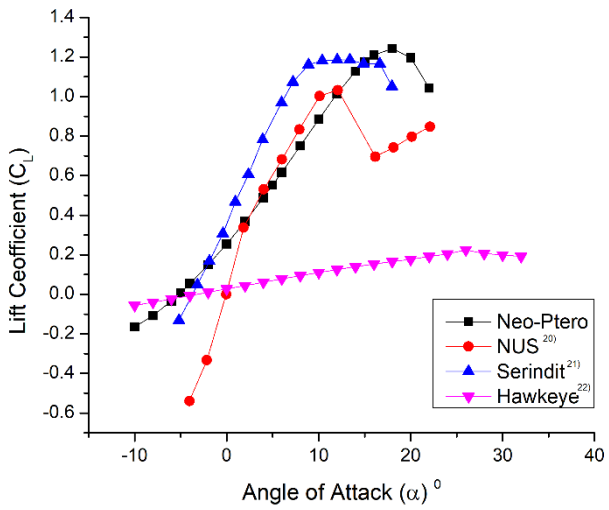

Fig. 10: C_L performances for Neo-Ptero alongside with NUS[20], Serindit[21] and Hawkeye[22] micro-UAV models.

Based on the overall C_L distribution, the results show that NUS and Serindit have slightly higher C_L generation than Neo-Ptero, particularly at α = 0° to 10°. The detailed analysis taken at the same α angle also shows that NUS and Serindit averagely produce at least 6% better C_L magnitude than Neo-Ptero. However, Neo-Ptero manages to induce six times higher C_L magnitude than Hawkeye at α = 0° to 10° on average.

The α range analysis is conducted on the basis of the beneficial lift distribution, which starts from the zero-lift angle of attack up to the stall angle. A larger α range magnitude means a better flight envelope, which extends the limiting flight condition boundaries for the micro-UAV model, and easy control without exceptional pilot skill[24]. Table 2 summarizes the magnitude of the α range for all models. The result shows that Neo-Ptero has at least a 17.6% wider α range magnitude compared with NUS and Serindit. Furthermore, Neo-Ptero has at least 38.5% higher stall angle than NUS and Serindit. Only Hawkeye has 30% wider α range magnitude and higher stall angle than the Neo-Ptero model.

In terms of C_{Lmax} magnitude, result shows that Neo-Ptero produces at least 5% better C_{Lmax} magnitude than the other micro-UAV models. Having a higher C_{Lmax} magnitude promisingly contributes in relaxing the need for low wing loading operation during takeoff, landing, and approach conditions[25]

Table 2. Summary of α range

micro-UAV model	C_L **parameters**			
	$\alpha_{CL=0}$	α_{stall}	**α range**	C_{Lmax}
Neo-Ptero	-2°	18°	20°	1.24
NUS	0°	11°	11°	1.06
Serindit	-4°	13°	17°	1.18
Hawkeye	0°	26°	26°	0.22

The drag performance of Neo-Ptero alongside the NUS[20], Serindit[21], and Hawkeye[22] micro-UAVs is presented in Fig. 11. In general, the C_D performance of the Neo-Ptero model is comparable with other micro-UAV models in terms of overall C_D curve trend, C_D magnitude, and percentage of C_D increment.

Based on the overall C_D curve trend, observation shows that Neo-Ptero induces a common C_D trend with other micro-UAV models. The C_D magnitude for all models starts at a low C_D magnitude and achieves its C_{Dmin} magnitude at α between -2° and 0°. As α increases, the C_D curves for every wing also continues to rise in magnitude. The common increment trend in C_D curves continuously seen in every wing as α angle rise beyond the stall angle. Despite the common C_D trend found between the models, the C_D curve for Neo-Ptero lies slightly higher than the other micro-UAV models, especially at α beyond 5°. Based on comparative analysis in C_D magnitude taken at α = 0° up to stall angle, Neo-Ptero induces at least 13.2% larger drag magnitude than the micro-UAV models on average. Larger C_D performance trend for Neo-Ptero continues in C_D increment magnitude. Neo-Ptero has

averagely induced at least 5% larger C_D increment than the other micro-UAV models for every 2° angle of attack increment between α = 0° to stall angle.

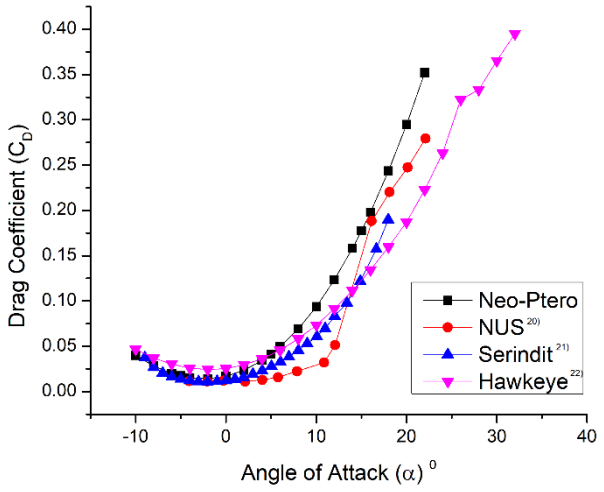

Fig. 11: C_D performances for Neo-Ptero alongside with NUS[20], Serindit[21] and Hawkeye[22] micro-UAV models.

Based on these C_D performance, Neo-Ptero has a larger drag penalty than the other models, particularly at an α angle beyond α = 0°. The significant C_D magnitude induced by Neo-Ptero that may affect its overall aerodynamic efficiency. Aerodynamic efficiency is an important performance parameter for UAVs to maximize its flight time and improve flight performance, such as maximum speed, stall speed, rate of climb, and turning radius[25].

4. Conclusion

Neo-Ptero is a tailless micro-UAV fully developed by IFCON (M) Sdn Bhd. Despite its successful prototyping development, the aerodynamic performance of the Neo-Ptero prototype remains unknown. Thus, this work aims to characterize the lift and drag distribution on the current Neo-Ptero prototype. The C_L analysis on Neo-Ptero shows that the model has a promising C_L performance throughout the α increment. For every 2° angle of attack increment, the model can generate approximately 22% increment in C_L magnitude. Neo-Ptero also has a decent magnitude in maximum lift coefficient and stall angle where it produces high C_{Lmax} and delayed α_{stall} at 1.24 and 18°, respectively. A C_L comparison study also reveals that Neo-Ptero has favorable C_L performances in terms of α range and C_{Lmax} magnitudes compared with NUS and Serindit. Neo-Ptero induces at least 17.6% and 5% better α range and C_{Lmax} magnitude, respectively, than those UAV models. Such C_L performance is beneficial to extending its flight envelope and relaxing the pilot control input during takeoff, landing, and approach conditions.

Based on C_D performance, Neo-Ptero does suffer from a severe C_D generation throughout the angle of attack increment. The model has produced an average of 23.8% rise in C_D magnitude for every 2° angle of attack increment. A comparative study on C_D performance found that Neo-Ptero induces at least 13.2% and 5% larger C_D magnitude and C_D increment, respectively, than the other micro-UAV models. Such C_D performance is considered Neo-Ptero's malevolent characteristics, which may further affect its overall aerodynamic efficiency and can limit its flight time and flight performances.

In future works, shape design improvement and wind tunnel works will be conducted to validate and enhance the aerodynamic performance of the current Neo-Ptero model.

Acknowledgements

The authors acknowledge technical and financial support from Universiti Teknologi MARA, Cawangan Pulau Pinang. Special gratitude is also given to the IFCON Technology (Malaysia) Private Limited Company, whose contribution in the funding the aircraft fabrications works. These works have been successfully accepted and presented at the event of MERD'20.

Nomenclature

μ	Micro
C_L	Lift coefficient
C_D	Drag coefficient
C_{Lmax}	Maximum lift coefficient
C_{Dmin}	Minimum drag coefficient
L	Total chordwise length
y+	y value of first cell
U_x	Velocity in x-direction
U_y	Velocity in y-direction
U	inlet velocity
α	angle of attack
$\alpha_{CL=0}$	zero-lift angle of attack
α_{stall}	stall angle

References

1) K. Gryte, R. Hann, M. Alam, J. Rohac, T.A. Johansen, and T.I. Fossen, "Aerodynamic modeling of the Skywalker X8 Fixed-Wing Unmanned Aerial Vehicle," in: 2018 International Conference on Unmanned Aircraft Systems, ICUAS 2018, Texas, USA, 2018: pp. 826–835. doi:10.1109/ICUAS.2018.8453370.
2) T.N. Dief, and S. Yoshida, "System identification for quad-rotor parameters using neural network," *Evergreen*, **3** (*1*) 6–11 (2016). doi:10.5109/1657380.
3) Z. Wang, M. Wen, S. Dang, L. Yu, and Y. Wang, "Trajectory design and resource allocation for uav

energy minimization in a rotary-wing uav-enabled wpcn," *Alexandria Engineering Journal*, **60** (*1*) 1787–1796 (2021). doi:10.1016/j.aej.2020.11.027.
4) T.N. Dief, and S. Yoshida, "System identification and adaptive control of mass-varying quad-rotor," *Evergreen*, **4** (*1*) 58–66 (2017). doi:10.5109/1808454.
5) K.P. Valavanis, and G.J. Vachtsevanos, "Handbook of unmanned aerial vehicles," *Handbook of Unmanned Aerial Vehicles*, 1–3022 (2015). doi:10.1007/978-90-481-9707-1.
6) B. Lee, P. Park, C. Kim, S. Yang, and S. Ahn, "Power managements of a hybrid electric propulsion system for uavs," *Journal of Mechanical Science and Technology*, **26** (*8*) 2291–2299 (2012). doi:10.1007/s12206-012-0601-6.
7) A. a. Paranjape, S.-J. Chung, H.H. Hilton, and A. Chakravarthy, "Dynamics and performance of tailless micro aerial vehicle with flexible articulated wings," *AIAA Journal*, **50** (*5*) 1177–1188 (2012). doi:10.2514/1.J051447.
8) N. Long, B. Millescamps, F. Pouget, A. Dumon, N. Lachaussée, and X. Bertin, "Accuracy Assessment of Coastal Topography Derived from UAV Images," in: International Archives of the Photogrammetry, Remote Sensing and Spatial Information Sciences - ISPRS Archives, Prague, Czech Republic, 2016: pp. 1127–1134. doi:10.5194/isprsarchives-XLI-B1-1127-2016.
9) S. Abudarag, R. Yagoub, H. Elfatih, and Z. Filipovic, "Computational analysis of unmanned aerial vehicle (UAV)," in: 2016 IEEE International Conference on Robotics and Automation (ICRA), Stockholm, Sweden, 2017: pp. 020001–10. doi:10.1063/1.4972593.
10) Y. Chen, H. Qi, G. Li, and Y. Lan, "Weed control effect of unmanned aerial vehicle (UAV) application in wheat field," in: International Journal of Precision Agricultural Aviation, 2018: pp. 25–31. doi:10.33440/j.ijpaa.20190202.45.
11) D.A. Lawrence, and B.B. Balsley, "High-resolution atmospheric sensing of multiple atmospheric variables using the datahawk small airborne measurement system," *Journal of Atmospheric and Oceanic Technology*, **30** (*10*) 2352–2366 (2013). doi:10.1175/JTECH-D-12-00089.1.
12) N.T.B. Hoang, and B. V. Bui, "Experimental and numerical studies of wingtip and downwash effects on horizontal tail," *Journal of Mechanical Science and Technology*, **33** (*2*) 649–659 (2019). doi:10.1007/s12206-019-0120-9.
13) N.I. Ismail, M.M. Mahadzir, A. Hasnul, M.A. Alias, A.A. Shariffuddin, and N.I. Kamel, "Development of neo-ptero tailless micro aircraft," *Journal of Engineering and Science Research*, **2** (*6*) 1–6 (2018). doi:10.26666/rmp.jesr.2018.6.1.
14) A. Klaptocz, and J. Nicoud, "Technology and Fabrication of Ultralight Micro-Aerial Vehicles," in: D. Floreano, J.-C. Zufferey, M. V. Srinivasan, C. Ellington (Eds.), Flying Insects and Robots, Springer Berlin Heidelberg, Berlin, Heidelberg, 2010: pp. 299–316. doi:10.1007/978-3-540-89393-6.
15) S. Barbarino, O. Bilgen, R.M. Ajaj, M.I. Friswell, and D.J. Inman, "A review of morphing aircraft," *Journal of Intelligent Material Systems and Structures*, **22** (*9*) 823–877 (2011). doi:10.1177/1045389X11414084.
16) V. Brusov, V. Petruchik, and Y. Tiumentsev, "Theoretical and experimental investigations of aerodynamics and flight dynamics for micro-uavs," *27th Congress of the International Council of the Aeronautical Sciences 2010, ICAS 2010*, **4** 3164–3172 (2010).
17) A.M. Halawa, B. Elhadidi, and S. Yoshida, "Aerodynamic performance enhancement using active flow control on du96-w-180 wind turbine airfoil," *Evergreen*, **5** (*1*) 16–24 (2018). doi:10.5109/1929723.
18) C.D. Harley, "Aerodynamic Performance of Low Form Factor Spoilers," PhD Thesis Dissertation, University of Manchester, 2010.
19) M.M. Takeyeldein, T.M. Lazim, N.A.R. Nik Mohd, I.S. Ishak, and E.A. Ali, "Wind turbine design using thin airfoil sd2030," *Evergreen*, **6** (*2*) 114–123 (2019). doi:10.5109/2321003.
20) C.S. Ming, "Unmanned Air Vehicle (UAV) Wing Design and Manufacture," Bachelor Thesis Dissertation, National University of Singapore, 2010.
21) K. Anuar, M. Akbar, and H. Herisiswanto, "Wing design of uav serindit v-1," in: IOP Conference Series: Materials Science and Engineering, 2019. doi:10.1088/1757-899X/539/1/012002.
22) M.S. Johari, Z.M. Ali, W. Wisnoe, N. Ismail, and I.S. Ishak, "Computational Aerodynamic Analysis Of UITM 's Hawkeye UAV Aircraft," in: International Symposium on Sustainable Aviation 2020, Selangor, Malaysia, 2020: pp. 1–5.
23) N.I. Ismail, H. Yusoff, H. Sharudin, A. Pahmi, H. Hafiz, and M.M. Mahadzir, "Lift distribution of washout twist morphing mav wing," *International Journal of Engineering & Technology*, **7** (*4.13*) 89–94 (2018).
24) M. V. Cook, "Flight Dynamics Principles," 2013. doi:10.1016/C2010-0-65889-5.
25) P. Panagiotou, and K. Yakinthos, "Aerodynamic efficiency and performance enhancement of fixed-wing uavs," *Aerospace Science and Technology*, **99** 105575 (2019). doi:10.1016/j.ast.2019.105575.